LEAN PREMIXED TURBULENT COMBUSTION MODELING USING FLAME TABULATED CHEMISTRY AND A PRESUMED PDF APPROACH

Julien Savre, Nicolas Bertier, Daniel Gaffie
Department of Fundamental and Applied Energetics,
ONERA
29, Avenue de la Division Leclerc, 92322 - Chatillon, France
julien.savre@onera.fr

Yves D'Angelo
INSA Rouen - CORIA,
CNRS UMR 6614
76801, Saint Etienne du Rouvray, France

ABSTRACT

A tabulated chemistry approach (FPI) is used within an LES context to compute the turbulent reacting flow inside a lean premixed swirl-burner. Chemical informations such as species reaction rates and species mass fractions are directly interpolated in the chemical database as a function of a unique progress variable. Furthermore, the effects of SGS fluctuations on the flame are accounted for using a presumed PDF approach (β-PDF), valid in the thin reaction zone regime. The evaluation of those PDFs requires the knowledge of the first two statistical moments of the progress variable (those two variables have thus to be modeled). The flow inside the model combustor is eventually successfully computed, and the profiles of averaged and RMS quantities are compared to experimental measurements. Using those comparisons, the ability of the model to predict pollutant species formation such as CO and CO_2 is assessed, and possible improvements of the model are discussed.

INTRODUCTION

During the past decade, large-eddy simulation (LES) has become a very useful and promising tool to model turbulent reacting flows inside complex geometries (Janicka and Sadiki, 2005; Pitsch, 2006). In particular, compared to RANS approaches, LES accounts for non-stationary flow effects that are particularly crucial to predict unsteady phenomena such as flame extinction, flame stabilization or pollutant emissions. For this latter point, a detailed description of chemical processes is also necessary to account for minor species production. Whereas detailed kinetic mechanisms are well known for the combustion of simple hydrocarbons such as CH_4, their direct use in LES of complex geometries is still out of reach because of the large amount of species balance equations that should be solved (the GRI-Mech 3.0 mechanism includes 56 species). Therefore, pollutant formation modeling using large-eddy simulation was only made possible by the development of chemistry reduction techniques such as ILDM (Maas and Pope, 1992) or, more recently, FPI (Gicquel et al., 2000). Those methods are mostly based on the construction of look-up tables where the chemical response of elementary combustion systems is lumped into a unique manifold as a function of a reduced number of progress variables. The original system consisting of N_{sp} independent variables (the number of species included in the kinetic mechanism) thus reduces to a N_c dimension problem,

where N_c is the number of progress variables.

A precise description of chemical phenomena is however not sufficient when addressing pollutant formation in turbulent reacting flows with LES, as the subgrid scale (SGS) fluctuations must also be accounted for. In LES indeed, the large scale turbulent structures are exactly resolved, whereas the influence of the small dissipative eddies must be modeled. Various models were proposed to account for the effects of SGS fluctuations on the flame dynamics and on species formation. Most of those approaches rely on the flamelet assumption which states that the turbulent flame structure remains locally similar to a laminar one (Peters, 2000).

The aim of the present study is to assess major pollutant species formation inside a model swirl-burner. In the experimental setup, studied by Meier et al. (2007), air and fuel are mixed inside the swirler, just before entering the combustor. Thus, a partially premixed flame develops in the chamber, stabilized by the large recirculating region created by the swirl motion. The flow being mainly piloted by those large structures, the combustion takes place within the thin reaction zone regime. Previous numerical studies (Roux et al., 2006; Galpin et al., 2008) showed that assuming a perfect mixing between fuel and air at the inlet of the chamber provides a good approximation of the flame characteristics. Considering this hypothesis, the FPI tabulation technique, based on laminar premixed flame computations, was retained as the best compromise to model detailed chemistry in LES computations of the burner. In addition, a presumed PDF approach was used as proposed by Vervisch et al. (2004), following the flamelet assumption. The PDF of the progress variable was then approximated by a β function, fully determined by the first two statistical moments of the progress variable. Hence, the key issue regarding turbulent combustion modeling resides in the evaluation of those two parameters.

In this work, we made use of the industrial CFD solver CEDRE, developed at the ONERA. It was shown previously by Savre et al. (2009) and Galpin et al. (2008) that the coupling between FPI and an industrial CFD code such as CEDRE is not straightforward and requires some major adaptations comparing to the original method employed for instance by Domingo et al. (2008). This issue was discussed in previous papers (Savre et al., 2009) and is out of the scope of the present study.

In the following, the modeling choices made concerning chemistry and turbulent combustion are first briefly de-

scribed. The computed swirl-combustor is then introduced and the numerical specificities of the simulations are given. In the next section, the different computations performed are detailed, and the results (mean temperature, CO and CO_2 mass fractions as well as RMS temperatures) are presented and discussed. The conclusions of the study and an introduction to the future works and possible improvements of the model are eventually exposed.

TURBULENT COMBUSTION MODELING

Chemistry

The FPI tabulation technique proposed by Gicquel et al. (2000) was retained to model detailed chemistry effects. under perfectly premixed conditions, the chemical response of a unique laminar unstrained freely propagating premixed flame computed using a dedicated solver (PREMIX) and detailed chemistry (GRI-Mech 3.0) is collected in a database according to its progress variable c. This latter is defined as the sum of CO and CO_2 mass fractions, normalized by its value at the equilibrium (so that c varies between 0 and 1). Then, in CFD simulations, the knowledge of c is sufficient to extract the corresponding values of $Y_i(c)$ and $\dot{\omega}_i(c)$ from the tables.

As stated earlier, the CEDRE CFD code (a cell-centered finite volume code dedicated to industrial applications and multiphysical flow modeling) was used in the present work. Two major ways of coupling FPI databases with a CFD software were distinguished by Galpin et al. (2008) and Savre et al. (2009) : basically, either all the species mass fractions are read in the tables, or major species mass fractions are transported, their chemical source terms being interpolated in the tables. Savre et al. (2009) showed that the specific architecture of CEDRE imposes the application of the second method. It was then established that this weak coupling between CEDRE and the FPI tables may induce important discrepancies within the computed flame structures. Those disparities may ultimately lead to burnt gas compositions different from the equilibrium. To overcome this issue, a correction model was proposed based on the relaxation of the interpolated reaction rates toward the tabulated manifolds. The chemical source terms $\dot{\omega}_i^*$ that should be used in the CFD code then read (Savre et al., 2009) :

$$\dot{\omega}_i^* = \dot{\omega}_i^{FPI} + \frac{Y_i^{FPI} - Y_i}{\tau_i} \tag{1}$$

where the superscript FPI denotes tabulated quantities and τ_i is a chemical time scale related to the ith species. It was shown that the best way to define this relaxation time scale is given by the reciprocal maximum value of the jacobian matrix diagonal term ($J_{ii} = \partial \dot{\omega}_i / \partial Y_i$) accross the flame. This model eventually ensures that the transported species mass fractions of the major species follow their tabulated trajectories in the phase space. Note that a different method was used by Galpin et al. (2008) in a similar context to determine the chemical reaction rates that has to be used in the CFD code from the tabulated data.

Flame/turbulence interactions

Flame behaviours may be dramatically modified by turbulent structures depending on the ratios between turbulence and flame characteristic time scales, which emphasizes the existence of distinct combustion regimes. At the moment, most of the existing turbulent combustion models are based on the flamelet hypothesis which presumes that the turbulent flame structure remains locally similar to a laminar one (the inner structure of the flame is not affected by the turbulent eddies). This assumption is supposed to remain true within the thin reaction zone regime, and supports the fact that laminar flame based tables may be used to describe turbulent premixed flames (Bradley et al., 1988) within this combustion regime.

In LES computations of flames in the flamelet regime, the laminar flame brush is usually thinner by an order of magnitude than the typical cell size so that all the interactions between the chemical reactions and the turbulent structures occur at the subgrid scale. In the present study, the SGS fluctuation effects on the flame front are accounted for using a presumed PDF approach (Vervisch et al., 2004). This model was already extensively validated within the framework of turbulent premixed combustion and it provides a very good compromise between accuracy and computational cost. Using the presumed PDF approach, the filtered chemical reaction rates may be obtained from the tabulated variables through :

$$\widetilde{\omega}_i = \int_0^1 \dot{\omega}_i^{FPI}(c) \, \widetilde{P}(c) \, dc \tag{2}$$

where $\widetilde{\cdot}$ denotes the favre filter operator. In our study, the PDF of the progress variable was given the shape of a β function (Bradley et al., 1988). This function is fully determined by the first two statistical moments of c, denoted $\widetilde{c}$ and $\widetilde{c''^2}$. It appears from relation 2, that this model is very well suited to tabulation techniques, as it enables the construction beforehand of filtered FPI databases. Those new tables, resulting from the application of equation 2, contain all the filtered quantities $\widetilde{Y}_i$ and $\widetilde{\omega}_c$ according to both input parameters $\widetilde{c}$ and $\widetilde{c''^2}$.

$\widetilde{c}$ and $\widetilde{c''^2}$ have then to be modeled. As the major species mass fraction balance equations are solved by the CFD code, $\widetilde{c}$ can be directly derived from its basic definition :

$$\widetilde{c} = \frac{\widetilde{Y}_{CO_2} + \widetilde{Y}_{CO}}{Y_{CO_2}^{eq} + Y_{CO}^{eq}} \tag{3}$$

Unlike $\widetilde{c}$, the SGS variance of c, defined by $\widetilde{c''^2} = \widetilde{c^2} - \widetilde{c}^2$, cannot be directly deduced from the transported quantities. However, a transport equation for this variable can be derived and reads (Domingo et al., 2005) :

$$\frac{\partial \overline{\rho}\widetilde{c''^2}}{\partial t} + \nabla.\left(\overline{\rho}\widetilde{u}\widetilde{c''^2}\right) = \nabla.\left(\overline{\rho}D_c\nabla\widetilde{c''^2}\right) \underbrace{-\nabla\tau_{c''^2}}_{I} \underbrace{-2\,\overline{\tau_c}\nabla\widetilde{c}}_{II}$$

$$\underbrace{-2\,\overline{\rho s_{\chi_c}}}_{III} + 2\overline{\rho}\underbrace{\left(\widetilde{\omega_c c} - \widetilde{\omega}_c\widetilde{c}\right)}_{IV} \tag{4}$$

Four unclosed terms appear in this equation. Term (I) and (II) represent respectively the SGS turbulent fluxes of $\widetilde{c''^2}$ and the contribution of the SGS turbulent fluxes of $\widetilde{c}$. Those two terms may be modeled using a simple gradient assumption : $\overline{\tau_{c''^2}} = -\overline{\rho}\frac{\nu_t}{Sc_t}\nabla\widetilde{c''^2}$ and $\overline{\tau_c} = -\overline{\rho}\frac{\nu_t}{Sc_t}\nabla\widetilde{c}$, where ν_t/Sc_t represents a turbulent diffusion coefficient, with ν_t and Sc_t given by the turbulence model (in this study, the Smagorinsky model was employed).

Term (III) expresses the subgrid progress variable dissipation rate. Its complete expression reads :

$$\widetilde{s_{\chi_c}} = \widetilde{\chi}_c - D\,|\nabla \widetilde{c}|^2 - 2D\widetilde{\nabla c''}.\nabla\widetilde{c} \qquad (5)$$

The last two terms of equation 5 are usually neglected compared with $\widetilde{\chi}_c$, so that the SGS progress variable dissipation rate is equivalent to the filtered dissipation rate (models for $\widetilde{\chi}_c$ are then easier to derive).

The most widely used model for $\widetilde{\chi}_c$ is the linear relaxation model. It is based on the assumption that $\widetilde{\chi}_c$ remains proportional to the inverse of a turbulence characteristic time scale. This hypothesis is somewhat too restrictive for a reactive scalar as it explicitly assumes that the dissipation of c is solely piloted by turbulent phenomena and is independent of the chemistry.

To include chemical effects in the modeling of the progress variable dissipation rate, Vervisch et al. (2004) proposed a model based on the BML assumption (under the BML limit, the flame front is supposed to be infinitely thin so that the PDF of c is characterized by a double delta shape). Following the bi-modal limit theory, it was shown by Bray and Moss (1977) that the scalar dissipation rate of c can be directly related to the progress variable reaction rate through :

$$\widetilde{\omega}_c = \frac{2}{2c_m - 1}\widetilde{\chi}_c \qquad (6)$$

$c_m = \widetilde{c\omega_c}/\widetilde{\omega}_c$ is a reaction weighted progress variable. Under the BML assumption, c_m tends to a constant value close to 0.75. Following equation 6, the scalar dissipation of c may be recast into the following form :

$$\widetilde{\chi}_c = \frac{C_1}{2}(2c_m - 1)\,\widetilde{\omega}_c \frac{\widetilde{c''^2}}{\widetilde{c}(1-\widetilde{c})} \qquad (7)$$

where we introduced a constant C_1 of the order unity. The additional factor $s = \widetilde{c''^2}/\widetilde{c}(1-\widetilde{c})$ (the segregation factor) was only introduced to verify the realizability condition on $\widetilde{\chi}_c$: $\widetilde{\chi}_c$ must indeed tend toward 0 when $s = 0$, and toward its BML value given by 6 when $s = 1$. This factor has hence no real physical sense but ensures a correct behaviour of $\widetilde{c''^2}$ when $\widetilde{\chi}_c$ is replaced in equation 4.

Finally, the progress variable reaction rate appearing in equation 7 should be further modeled. By introducing the flame surface density function $\Sigma = \overline{|\nabla c|}$, one may relate $\widetilde{\omega}_c$ to Σ through the relation : $\overline{\rho}\widetilde{\omega}_c \approx \rho^0 S_L^0 \Sigma$, with ρ^0 the fresh gas density, and S_L^0 the unstrained laminar flame speed (the effects of strain and curvature on the flame speed are neglected). To avoid the resolution of an extra balance equation for the flame surface density, Σ may be modeled using $\Sigma \approx \Xi\,|\nabla\widetilde{c}|$, so that one may find :

$$\overline{\rho}\widetilde{\omega}_c \approx \rho^0 S_L^0 \Xi\,|\nabla\widetilde{c}| \qquad (8)$$

The coefficient Ξ is called the wrinkling factor. Several algebraic relations were developed to provide a simple closure for this coefficient, as a function of the ratios between the subgrid scales of turbulence and the flame characteristic scales. We retained in this study the model proposed by Peters (2000) :

$$\Xi = 1 - C_A\left(\frac{\Delta}{\delta_L^0}\right) + \sqrt{\left(\frac{C_B \Delta}{\delta_L^0}\right)^2 + C_C\left(\frac{u'\Delta}{S_L^0 \delta_L^0}\right)} \qquad (9)$$

where Δ denotes the filter size, δ_L^0 is the unstrained laminar flame thickness and u' is a characteristic subgrid velocity

fluctuation. C_A, C_B and C_C are three constants respectively equal to 0.52, 0.195 and 0.78.

The last unclosed term in equation 4 (term (IV)) expresses a reactive correlation : $\widetilde{\omega_c c} - \widetilde{\omega}_c\widetilde{c} = \widetilde{\omega_c c''}$. This term is usually closed using the tabulated data, which implies that $\widetilde{\omega_c c}$ must necessarily be *a priori* computed using integral 2, and tabulated. This term is then interpolated in the database as a function of the first two statistical moments of c.

Note that this model, used by Domingo et al. (2008) in previous computations, seems not fully satisfactory. The introduction of this model in equation 4 leads indeed to an implicit relation, as $\widetilde{\omega_c c''}$ depends directly on the SGS variance of c. The exact resolution of the system should thus require an iterative procedure that would demand extra computational resources in LES computations. In the present work, this model based on the use of tabulated quantities was employed however, but this discussion stresses the need in developing a new model for $\widetilde{\omega_c c''}$.

The four unclosed terms appearing in equation 4 are now modeled, and the equation can be solved as such. Further simplifications of equation 4 may however lead to an even simpler and more practical model for $\widetilde{c''^2}$. Indeed, if we assume the balance between production (terms (II) and (IV)) and dissipation (term (II)), an algebraic closure for $\widetilde{c''^2}$ can be derived. This relation reads :

$$\widetilde{c''^2} = \frac{2C_2}{2c_m - 1}\frac{\overline{\rho}\widetilde{c}(1-\widetilde{c})}{\rho_0 S_L^0 \Xi\,|\nabla\widetilde{c}|}\left[\frac{\nu_t}{Sc_t}\,|\nabla\widetilde{c}|^2 + \widetilde{\omega_c c''}\right] \qquad (10)$$

Previous studies using this model showed that $C_2 = 1$ seems appropriate. In this work, the algebraic relation 10 was used which avoids the solving for an additional balance equation for $\widetilde{c''^2}$.

As well as for the laminar case, the filtered species reaction rates extracted from the FPI databases during the CFD computations have to be corrected prior to be replaced in the filtered balance equations. As explained earlier, the weak indirect coupling imposed between the FPI tables and CEDRE may induce huge discrepancies within the computed flames leading to unrealistic equilibrium compositions. To avoid this, a relation similar to equation 1 must be used. As a first order closure, the same relation as 1 may be employed in the turbulent context, where the laminar quantities are replaced by filtered quantities. This model enables a correct relaxation of the transported species toward their tabulated trajectories, but at a probably unaccurate rate. Actually, the relaxation time scale imposed in relation 1 corresponds to a purely chemical time scale which does not account for external perturbing phenomena such as turbulence. Turbulent characteristic time scales should hence be taken into account here, either by a redefinition of the relaxation time scale, or by a simple correction of the existing one (Teraji et al., 2009).

DESCRIPTION OF THE COMBUSTOR SIMULATIONS

The model swirl-burner
In the initial burner configuration, an inflow of pure air under atmospheric conditions ($P = 1\ atm$, $T = 300\ K$) is injected via a plenum in the combustor through the 12 radial chanels of the swirler. The mass flow rate of the inlet air flow is about 734.2 g/min. The fuel (CH_4) is injected

Sixth International Symposium on Turbulence and Shear Flow Phenomena
Seoul, Korea, 22-24 June 2009

within the swirler, through 12 holes measuring 1 mm in diameter. Thus, a partial premixing of fuel and air enters the combustion chamber through an exit nozzle of 27.85 mm in diameter. Then, a partially premixed flame develops in the chamber, stabilized by the precessing vortex core (PVC) resulting from the rotation of the flow. The chamber possesses a 85×85 mm square section and is 114 mm long.

3 different flames were experimentally studied, exhibiting quite different behaviours. The case retained in this work is the only case where a stable flame was observed. Here, the fuel is injected with a mass flow rate of 35.9 g/min, which corresponds to a mean equivalence ratio of 0.83.

The combustion chamber was equipped with optical access, so that measurements of species concentrations through Raman scattering or LIF were possible. Measurements of velocity were also performed using LDV, but under slightly different initial conditions, at $\Phi = 0.75$.

Details on the simulations

For modeling reasons, the initial configuration presented previously was slightly modified for the needs of the computations. Instead of injecting the fuel and the air separately, a perfect methane/air mixture is directly injected at the inlet, before the plenum, and the small fuel injection holes are suppressed of the geometry. Previous computations on this perfectly premixed configuration (Roux et al., 2006; Galpin et al., 2008) proved that this raw simplification does not significantly affect the description of the dynamics and properties of the flame.

A large box representing the atmosphere surrounding the device was added to the combustor in order to avoid spurious acoustic wave reflexions inside the computational domain (see figure 1). In addition, non reflecting outlets were imposed around this box, except for the upstream section where a slow coflow of air was imposed to avoid numerical difficulties. At the inlet, a small part of the injection chanel was retained in the computational domain. It was shown after several tests, that the length of this chanel plays a key role in the dynamics of the simulated flame. Modifying the length of this part affects the acoustic modes of the chamber which might lead to strong combustion instabilities. The length of the present chanel (50 mm)was determined so that no flame instabilities are observed. At the inlet, the total mass flow rate and the mixture composition and temperature are imposed. The other limits of the domain are supposed to be adiabatic walls.
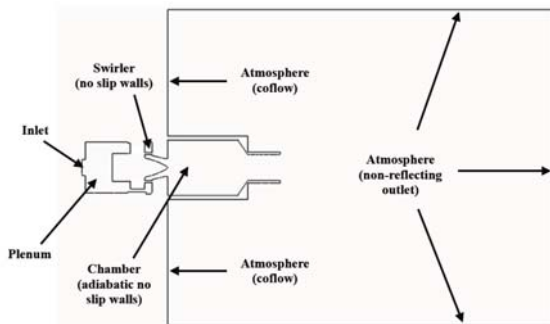
Figure 1: schematic representation of the computational domain.

Simulations were performed on two different fully unstructured 3D meshes in order to check the influence of grid refinement. The coarse grid includes about $1,750,000$ cells ($3,500,000$ faces), whereas the refined grid contains about $2,900,000$ cells ($5,500,000$ faces). The smallest cells in each grid were located inside the flame region, and their equivalent diamaters were evaluated respectively at 3 mm and 1.5 mm. Computations on the refined grid are still in progress because the physical time simulated up to now is not yet sufficient to provide converged RMS quantities (but the mean quantities are shown in the following).

CEDRE uses a cell-centered finite volume approach, with a MUSCL type second order scheme and Roe fluxes. The time integration was performed using a second order Runge-Kutta explicit scheme. The time-step used in each computation was deduced from the CFL criterion (for the RK2, $\frac{|u+c|\Delta t}{\Delta x} < 0.5$). Using this definition, the time steps for each case were respectively set to $1.2e-7$ s and $6e-8$ s.

Finally, the LES simulations were performed using the Smagorinsky model and the filtered FPI databases were meshed using 250 points along the $\widetilde{c}$ direction and 30 points along $\widetilde{c''^2}$.

RESULTS

The computed results are compared to the experimental measurements of Meier et al. (2007) and RANS $k - \epsilon$ results performed on the same grid with a simplified one-equation chemistry. The profiles are plotted for five different locations accross the combustor, at 6 mm, 10 mm, 20 mm, 40 mm and 80 mm. Mean quantities are obtained by averaging the LES results over a physical time of 26 ms on the coarse grid and 11 ms on the refined grid.

Mean temperature and CO_2 mass fractions

Figures 2 and 3 depict the mean temperature and CO_2 mass fraction profiles. Computed profiles of temperature exhibit over-estimated levels close to the walls, especially at $h = 6$ mm and $h = 10$ mm. This can be attributed to the adiabatic wall assumption that does not reflect the effects of heat losses at the wall on the temperature distribution in the combustor.
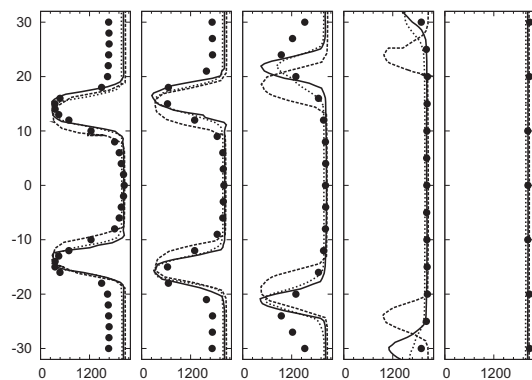
Figure 2: Mean temperature profiles (K) as a function of the radius (mm). From left to right : $h = 6$ mm, $h = 10$ mm, $h = 20$ mm, $h = 40$ mm and $h = 80$ mm. Symbols, experiment, full lines, LES coarse mesh, dotted lines, LES refined mesh, dashed lines, RANS.

The flame spread in the chamber is particularly well reproduced by the LES simulations. On the opposite, the RANS simulation tends to largely under-predict the flame angle, which leads to very poor agreements considering temperature and $\widetilde{Y_{CO_2}}$ profiles downstream. The flow field and the interactions between turbulence and chemistry are, in

438
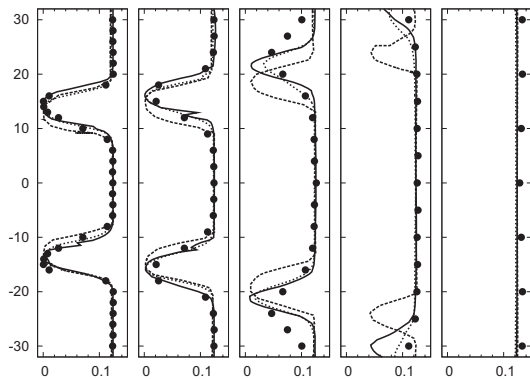
Figure 3: Mean Y_{CO_2} mass fractions profiles as a function of the radius (mm). From left to right : $h = 6\ mm$, $h = 10\ mm$, $h = 20\ mm$, $h = 40\ mm$ and $h = 80\ mm$. Symbols, experiment, full lines, LES coarse mesh, dotted lines, LES refined mesh, dashed lines, RANS.

this test case, essentially piloted by the large turbulent eddies created by the swirler. This explains why, within this context, the LES, which resolves exactly the large structures of the flow, clearly outperforms RANS approaches.

Close to the swirler exit, temperature and $\widetilde{Y_{CO_2}}$ profiles show that the mean flame brush thickness is still underpredicted by the LES (particularly at $h = 20\ mm$). Those results could easily be improved by increasing the progress variable SGS variance in the computation. The model constant C_2 appearing in relation 10 (the SGS variance algebraic formulation) may hence be set to 2. Further downstream, at $h = 20\ mm$ and $h = 40\ mm$, the refined mesh tends to predict minimum temperature and $\widetilde{Y_{CO_2}}$ levels closer to experimental measurements than the coarse grid.

Mean CO mass fractions

The implementation of FPI in the CFD solver CEDRE must enable an accurate description of pollutant formation inside industrial type combustion chambers. It is thus particularly interesting to check the ability of the developed approach to predict carbon monoxide formation within the model combustor. $\widetilde{Y_{CO}}$ profiles are ploted on figure 4. Close to the swirler exit, the computed profiles exhibit a well pronounced double peak shape which is not observed on the experimental measurements. However, the first computed CO peak matches perfectly the experimental peak, with a maximum of about 0.01 (note that experimental uncertainties on CO levels may be as high as 50%). The absence of a second peak on CO measurements may be explained by the mixing of the flame with burnt gases recirculating in this region of the chamber. The FPI model used in those computations is not able to account for this dilution because only one elementary flame with fixed equivalence ratio was tabulated. One can however expect bidimensional FPI databases, built using laminar premixed flame calculations with varying equivalence ratios and parametrized by both the progress variable and a mixture fraction, to give results closer to the experimental observations.

At $h = 40\ mm$, the predicted flow is more homogeneous and the double peak has disappeared. The coarse grid tends to over-estimate the maximum level of $\widetilde{Y_{CO}}$ reached at this position whereas the refined grid gives more realistic results. On the last profile, one can notice that the flow is fully homogeneous and a quasi constant CO level is observed. The levels given by the refined grid are globally in a good
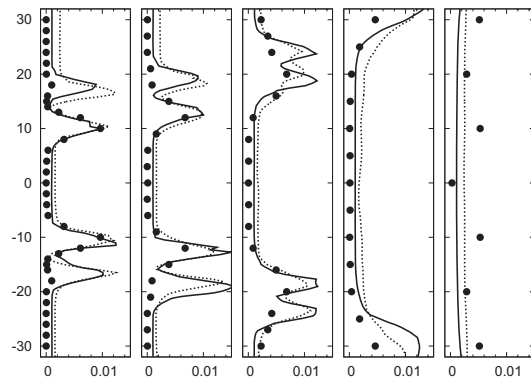
Figure 4: Mean Y_{CO} mass fractions profiles as a function of the radius (mm). From left to right : $h = 6\ mm$, $h = 10\ mm$, $h = 20\ mm$, $h = 40\ mm$ and $h = 80\ mm$. Symbols, experiment, full lines, LES coarse mesh, dotted lines, LES refined mesh.

agreement with the experimental results whereas the coarse grid tends to under-estimate them.

Temperature fluctuations

Profiles of temperature fluctuations are depicted on figure 5. LES results obtained on the refined grid are not shown here because the RMS quantities are not yet converged and still exhibit uncorrect behaviours.
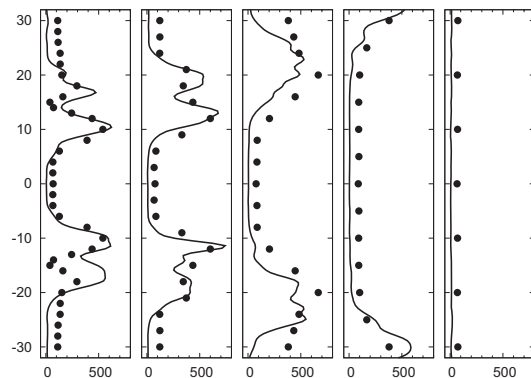
Figure 5: RMS of temperature profiles (K) as a function of the radius (mm). From left to right : $h = 6\ mm$, $h = 10\ mm$, $h = 20\ mm$, $h = 40\ mm$ and $h = 80\ mm$. Symbols, experiment, full lines, LES coarse mesh.

RMS quantities are usually particularly discriminating when considering LES simulations. In the present case, the overall shape of the profiles is correctly retrived by the LES, with a clear double peak shape upstream the chamber. T_{RMS} levels are also very accurately predicted by the simulation. However a slight under-estimation of the T_{RMS} predicted by the model is observed in the burnt gases, which could be attributed to heat losses effects or measurements uncertainties. Moreover, it should be noticed that close to the nozzle exit, the second peak predicted by the calculation is over-estimated.

Actually, grid refinement is expected to have significant effects on the computed T_{rms} profiles. Veynante and Knikker (2006) proved indeed that the size of the LES filter is really crucial to predict correct resolved RMS quantities. When the LES results obtained with the refined grid will be averaged on a sufficiently long physical time, the role of

the mesh resolution on the RMS levels will be further discussed. In addition, it is important to stress that the RMS temperatures ploted on figure 5 only correspond to resolved quantities. Subgrid fluctuations might actually have a significant contribution to the overall RMS quantities and should deserve further investigations (Veynante and Knikker, 2006).

CONCLUSIONS AND FUTURE WORKS

A new coupling method between CFD codes and chemical tables recently proposed by Galpin et al. (2008) and Savre et al. (2009) was applied to the LES of a lean premixed swirled burner. The model combustor is assumed to operate under perfectly premixed conditions so that the FPI model of Gicquel et al. (2000) may be used to create one-dimensional chemical tables parametrized by the progress variable c. This approach must allow detailed chemistry simulations for low computational costs, so that pollutant formation inside the swirled burner can be studied.

The FPI databases, providing the chemical source terms of the transported species in the CFD code, are used in conjunction with a presumed PDF approach to model turbulence/chemistry interactions. As the studied model combustor lies within the thin reaction zone regime, β-PDFs were retained that are fully determined by the first two statistical moments of the progress variable. The SGS variance of c especially requires some specific modeling. In this work, an algebraic closure for $\widetilde{c''^2}$ was proposed, based on the SGS scalar dissipation model of Vervisch et al. (2004), and production/dissipation balance hypothesis.

The LES results presented in this paper exhibited some particularly interesting features. First, it was shown that the flame angle at the exit of the swirler is perfectly predicted by the LES computations. This leads to excellent overall agreements between computed and measured profiles of mean temperature and CO_2 mass fraction. The profile comparisons however reveal that the mean flame brush thickness is slightly under-estimated upstream, which could be corrected by increasing the modeled progress variable SGS variance. When considering mean CO mass fraction profiles, a double peak shape is observed in the computations close to the swirler exit whereas the experimental measurements exhibit just a single peak. This behaviour can be attributed to the dilution of the flame by the recirculating hot gases in the upper side of the combustor. Indeed, this phenomenon cannot be accounted for by the present model as the FPI table was only built for perfectly premixed combustion. The level of the maximum CO mass fraction reached accross the flame is however well reproduced which is particularly encouraging regarding the ability of the model to accurately predict pollutant formation inside complex geometries. Finally, RMS of temperature were correctly predicted by the FPI computations. However, grid resolution is expected to have a significant impact on the computed RMS quantities. The exact role played by the mesh will be further discussed when RMS quantities obtained with the refined grid will be available.

In the near future, computations of the swirled combustor using FPI will be pursued on the fine grid. On a long term basis, we intend to account for dilution and partial premixing effects by constructing bidimensional FPI tables parametrized by c and a mixture fraction z.

REFERENCES

Janicka, J., Sadiki, A., 2005, "Large Eddy Simulation of

Turbulent Combustion Systems," *Proceedings of the Combustion Institute*, Vol. 30, pp. 537-547.

Pitsch, H., 2006, "Large-Eddy Simulation of Turbulent Combustion", *Annual Review of Fluid Mechanics*, Vol. 38, pp. 453-482.

Smith, G.P., Golden, D.M., Frenklach, M., Moriarty, N.W., Eiteneer, B., Goldenberg, M., Bowman, C.T., Hanson, R.K., Song, S., Gardiner, W.C., Lissianski, V.V., Qin, Z., "Gri-mech 3.0", *Technical Report, http://www.me.berkley.edu/gri-mech/.*

Maas, U., Pope, S.B., 1992, "Simplifying Chemical Kinetics : Intrinsic Low-Dimensional Manifolds in Composition Space", *Combustion & Flame*, Vol. 88, pp. 239-264.

Gicquel, O., Darabiha, N., Thevenin, D., 2000, "Laminar Premixed Hydrogen/Air Counterflow Flame Simulations Using Flame Prolongation of ILDM with Differential Diffusion, *Proceedings of the Combustion Institute*, Vol. 28, pp. 1901-1908.

Peters, N., 2000, "Turbulent Combustion", Cambridge University Press

Vervisch, L., Hauguel, R., Domingo, P., Rullaud, M., 2004, "Three Facets of Turbulent Combustion Modeling : DNS of Premixed V-Flame, LES of Lifted Non-Premixed Flame and RANS of Jet-Flame", *Journal of Turbulence*, Vol. 5, pp. 1-36.

Meier, W., Weigand, P., Duan, X.R., Giezendanner-Thoben, R., 2007, "Detailed Characterization of the Dynamics of Thermoacoustic Pulsations in a Lean Premixed Swirl Flame", *Combustion & Flame*, Vol. 150, pp. 2-26.

Roux, S., Lartigue, G., Poinsot, T., Meier, U., Berat, C., 2005, "Studies of Mean and Unsteady Flow in a Swirled Combustor Using Experiments, Acoustic Analysis, and Large-Eddy Simulations", *Combustion & Flame*, Vol. 141, pp. 40-54.

Galpin, J., Naudin, A., Vervisch, L., Angelberger, C., Colin, O., Domingo, P., 2008, "Large-Eddy Simulation of a Fuel-Lean Premixed Turbulent Swirl-Burner", *Combustion & Flame*, Vol. 155, pp. 247-266.

Domingo, P., Vervisch, L., Veynante, D., 2008, "Large Eddy Simulation of a Lifted Methane Jet Flame in a Vitiated Coflow", *Combustion & Flame*, Vol. 152, pp. 415-432.

Savre, J., Bertier, N., Gaffie, D., D'Angelo, Y., 2009, "Computations of Laminar Premixed Flames Using Extended FPI Modeling", *Proceedings of the European Combustion Meeting.*

Bradley, D., Kwa, L.K., Lau, A.K.C., Missaghi, M., Chin, S.B., 1988, "Laminar Flamelet Modeling of recirculating Premixed Methane and Propane-Air Combustion", *Combustion & Flame*, Vol. 71, pp. 109-122.

Domingo, P., Vervisch, L., Payet, S., Hauguel, R., 2005, "DNS of a Premixed Turbulent V-Flame and LES of a Ducted Flame Using a FSD-PDF Subgrid Scale Closure with FPI Tabulated Chemistry", *Combustion & Flame*, Vol. 143, pp. 566-586.

Bray, K.N.C., Moss, J.B., 1977, "A Unified Statistical Model of the Premixed Turbulent Flames", *Acta Astronautica*

Teraji, A., Imaoka, Y., Tsuda, T., Noda, T., Kubo, M., Kimura, S., 2009, "Development of a Time-Scale Interaction Combustion Model and its Application to Gasoline and Diesel Engines", *Proceedings of the Combustion Institute*, In Press.

Veynante, D., Knikker, R., 2006, "Comparison Between LES Results and Experimental Data in Reacting Flows", *Journal of Turbulence*, Vol. 7